15th IFK
Proc. of the 15th International Fluid Power Conference <Symposium/Conference>
<DOI>

Influence of Fluid Mechanical Properties of Hydraulic Oils with Different Chemical Structures on the Efficiency of Hydraulic System Components

Sebastian Deuster, Marius Hofmeister, Faras Brumand-Poor, Katharina Schmitz

RWTH Aachen University - Institute for Fluid Power Drives and Systems (ifas), sebastian.deuster@ifas.rwth-aachen.de

Abstract.

This paper aims to describe the influence of synthetic fluids from Group 5 on various system boundaries and components of hydraulic systems, and to compare them with conventional hydraulic mineral oil. The focus is on evaluating the fluid mechanical properties. For this purpose, losses in pumps and pipes, as well as in valves, are analysed. Initially, these components are investigated and modelled mathematically to obtain a fundamental understanding. Experimental tests were conducted on a real hydraulic system of a mobile working machine using two different types of hydraulic fluids. These fluids include a mineral oil-based HLP (Group 2), a synthetic ester HEES (Group 5). The fluids are compared based on system boundaries losses in hydraulic systems components. The influence of their different chemical and physical properties is discussed.
The paper concludes with an analysis of the influence of the different losses when using alternative hydraulic fluids compared to mineral oils in hydraulic systems and potential future research activities in this field.

Keywords. Alternative hydraulic fluids, loss mechanism, energy efficiency, mobile machinery.

1. INTRODUCTION

In addition to the mechanical components of a hydraulic system, the hydraulic fluid is a key component that plays a crucial role in the efficiency and operating behavior of hydraulic machines. Hydraulic fluids consist mainly of a base oil and a small proportion of additives. Different base oils can result in varying chemical and physical properties. Base oils are classified according to the American Petroleum Institute (API). The API classifies base oils into five groups. Groups 1 to 3 include mineral oils of varying purity. Groups 4 and 5 comprise fully synthetic base oils. Most lubricants are based on mineral oils from Groups 1 to 3. Their market share is approximately 85%, with synthetic base oils accounting for 15 % [1]. Synthetic base oils, such as esters or polyalphaolefins, offer, for example, the advantage

of adapting physical properties, including viscosity-temperature behavior, to the respective conditions of the hydraulic system during operation. Due to higher acquisition costs and the lack of suitable application tools for designing hydraulic systems tailored to a specific system, market sales are low compared to conventional mineral oils.

However, the use of hydraulic fluids based on API group 4 to 5 base oils has increased significantly in recent years [2]. These synthetic base oils provide physical and chemical properties that differ significantly, in some cases, from those of conventional mineral oils (Group 2). Using these oils in hydraulic systems results in distinct fluid mechanical and thermodynamic properties during their operation.

Previous research focused on the performance characteristics of synthetic hydraulic fluids in hydraulic displacement units [3, 4], which showed that the use of synthetic hydraulic fluids results in different efficiency levels than those achieved with conventional mineral oils. The tribological behaviour of synthetic esters was investigated in greater depth in comparison with mineral oils by [5, 6]. It was found that friction losses and wear are higher when synthetic esters are used. Jakobs [7] demonstrated in his work that the use of synthetic esters results in differentiated switching behaviour compared to mineral oils.

Previous work by us [8] showed high deviations in the overall efficiency of a mobile machine when using water-based hydraulic fluids instead of mineral oils.

This paper aims to expand on this work by identifying the causes of efficiency differences and balancing energy losses in the components of the hydraulic system. Unlike previous work, the focus here is on comparing mineral oils and synthetic esters.

The work is structured as follows: First, the fluid properties of the hydraulic fluid under investigation, mineral oil and synthetic esters, are presented in a comparative manner. This is followed by a presentation of the mathematical principles relating to the loss mechanisms that occur during the operation of a mobile machine. Particular attention is paid to the influence of different physical properties between mineral oils and synthetic esters. This is followed by validation of the mathematical assumptions using experimental data from a test excavator. The system is divided into different boundaries. Furthermore, the total losses during a dig and dump cycle of the machine, operating with different hydraulic fluids, are presented. Finally, a summary is provided in which the question should be answered: Which losses in the system are responsible for the different energy requirements associated with the use of different fluids in a mobile working machine?

2. FLUID PROPERTIES

The use of alternative lubricants results in variations in physical properties, which affect their operating behaviour when used in components and machines. Compared to conventional hydraulic fluids based on mineral oils, it is primarily the chemical structure of the base fluids that is responsible for differences in physical properties such as viscosity behaviour or density. Additives for hydraulic applications are used in nearly all base oil groups, featuring similar chemical components. These correlations can only be used qualitatively in the development of lubricants in the form of predictions and cannot be applied in a targeted manner by now.

The hydraulic fluids considered for the experimental investigations in this work differ fundamentally in their base fluid structure. This chapter examines the chemical structure of various base oils and explains the resulting physical properties.

2.1. Rheology and chemical structure

Viscosity generally describes the thickness of a fluid. It is used as a measure of a liquid's internal friction. This internal friction arises between the molecules of a flowing medium [9]. Physically, viscosity can be derived using the relationships shown in **Figure 2.1**. A fluid element located between a wall and a plate parallel to it is displaced by a force F applied on the plate. This creates a velocity gradient $d\dot{x}$ to the fluid between the moving plate and the stationary wall. The resulting shear stress τ depends on the area A of the moving plate.

The dynamic viscosity η is defined for Newtonian fluids as the proportionality constant between the shear rate $\dot{\gamma}$ and the shear stress τ acting on the fluid.

Figure 2.1 b) shows the atomic relationships for the graphical representation of the viscosity of lubricants in general. Molecular chains of hydrocarbons slide over each other due to an initiating force. The positively charged nuclei of the molecules repel each other due to their identical charge. For molecules to move from a given location to a vacant space, they must overcome a potential barrier. This requires activation energy. The potential barrier described defines the viscosity of the fluid. Additionally, mechanical resistance is caused by the branching of molecular chains and by branching structures within the chains. [10]

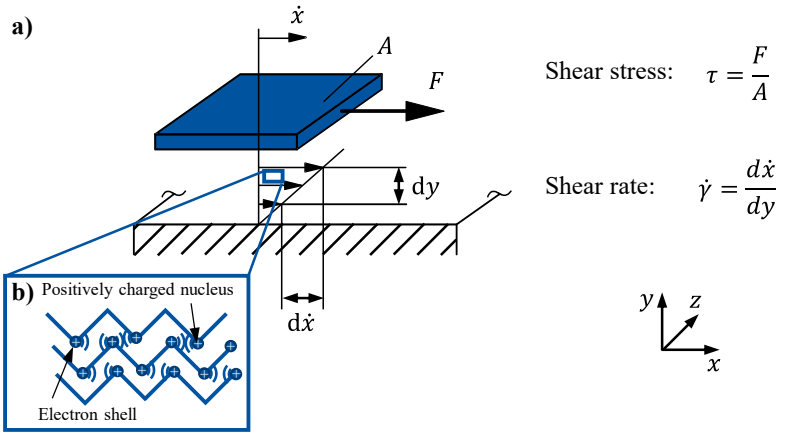

Figure 2.1. (a) Derivation of dynamic viscosity and (b) Intermolecular interactions between hydrocarbon chains in lubricants to illustrate viscosity at the atomic level

The base oils of the hydraulic fluids considered in this paper differ in their chemical structure. The differences in structure between mineral oils and esters primarily lie in the extent of branching and side chains. The chain length of the hydrocarbon chains, on the other hand, is similar for both types. Esters usually have long linear aliphatic molecular chains, whereas mineral oils have inflexible structural elements in the form of side chains. This difference in chemical structure influences the viscosity behavior of hydraulic fluids depending on temperature and pressure. Furthermore, this means that the carbon chains in ester oils are located nearer to each other, resulting in a higher packing capacity and thus a

higher density of ester oils compared to mineral oils. These relationships will be examined in more detail in the following chapters.

2.2. Temperature-viscosity behaviour

The viscosity of hydraulic fluids is highly dependent on temperature. As the temperature rises, the viscosity of the fluid decreases. At the microscopic level, this behavior can be explained as follows: Temperature affects the vibration and changing speeds of the atoms and molecules in the lubricant. The resulting vibration-energy reduces the activation energy required to overcome the potential barrier (see Figure 2.1). Corresponding mathematical descriptions of this behavior take the form of the Arrhenius equation [10]. Viscosity-temperature behavior depends on the chemical structure of the base fluid. Flexible, long linear molecular chains, such as esters, exhibit the lowest temperature dependence of viscosity. Inflexible structural elements, such as branches or sidechains, like in mineral oils, increase the dependence of viscosity on temperature accordingly [11]. Branching causes the hydrocarbon chains to separate further apart spatially, thereby reducing their influence compared to closely linked chains. The degree of dependence of viscosity on temperature is described using the viscosity index. As the viscosity index (VI) increases, the dependence of viscosity on temperature decreases. The calculation basis for determining the VI is described in DIN ISO 2909 [12]. While the VI of mineral oils is typically around 100, ester-based oils achieve values exceeding 180 [13].

2.3. Pressure-viscosity behaviour

The pressure-viscosity behavior is a fluid-specific characteristic that depends mainly on the composition of the base fluid. The addition of additives has a negligible influence. The pressure-viscosity behavior generally increases with the degree of branching, the number of cyclic structures, the presence of aromatic compounds, and the length of the side chains of the base oil (see **Fehler! Verweisquelle konnte nicht gefunden werden.**). Both naphthenic and paraffinic-based mineral oils have pronounced branched chain structures. These structures intertwine under increasing pressure, which in turn increases the internal friction within the fluid. Ester molecules have a significantly flatter structure with few side structures. This results in a lower pressure dependence on the viscosity. [14]

There are several approaches to calculating viscosity-pressure behavior. The first and still current approach is that, according to Barus (Eq. 2.1) [15]. Here, the dynamic viscosity η_0 at a specific pair of values for temperature and atmospheric pressure is the initial value. For a pressure p, the pressure-dependent dynamic viscosity $\eta(p)$ is determined. α_η is the pressure-viscosity coefficient, which is determined experimentally. The pressure-viscosity coefficient depends on the fluid and as described above, is largely determined by the chemical structure of the base oil. The coefficient for ester-based oils is therefore lower than for naphthenic mineral oils.

$$A_0 = \frac{\mu_0 \omega I_0}{4\pi} = 10^{-7} \omega I_0 \eta_0 \cdot e^{(\alpha_\eta \cdot p)} \quad (2.1)$$

Due to the exponential relationship, the pressure-viscosity coefficient (pV-Coefficient) and, thus, the use of different base oils have a significant influence on the viscosity of the lubricant in highly loaded tribological contacts. Studies in [16] show that the influence of the pressure-viscosity behavior is decisive for the formation of a load-bearing lubricating film and is only influenced to a small extent by the temperature-viscosity behavior.

2.4. Fluids investigated

The hydraulic fluids used in this study are a naphthenic mineral oil (HLP 46) and a synthetic ester (HEES 46) with a minimum content of 25 % renewable raw materials. It is a biobased lubricant in accordance with DIN 16807 [17]. Both fluids are commercially available hydraulic fluids containing additives. Table **2.1** shows the most important physical properties of the hydraulic fluids considered in this paper.

Table 2.1. Physical properties of the investigated hydraulic fluids

Fluid	Viscosity index	Density (15 °C) [kg/m³]	Spec. heat capacity [kJ/(kg·K)]	Therm. conductivity [W/(m·K)]	pV-coefficient [10^{-3}bar^{-1}]
HLP 46	113	858	2.0	0.135	2.0
HEES 46	184	944	2.3	0.14	1.5

3. MATHEMATICAL FUNDAMENTALS OF LOSS MECHANISMS IN HYDRAULIC SYSTEMS

This section presents a mathematical analysis of various common hydraulic components in terms of their losses resulting from fluid properties, which are eventually utilized for the examination of the experimental investigations.

3.1. Flow Friction

The hydrostatic and hydrodynamic pressure drops of the pipe and the orifice, as well as the tribological contacts in a pump, are investigated. Regarding the pipe, an advanced description of the relationship between laminar volumetric flow rate and pressure drop is provided by computing both steady-state and transient relations. The steady relation is determined by the Hagen-Poiseuille law:

$$\mathrm{A}_0 = \frac{\mu_0 \omega \mathrm{I}_0}{4\pi} = 10^{-7} \omega \mathrm{I}_0 \frac{\boldsymbol{\pi R^4}}{\boldsymbol{8\eta L}} \boldsymbol{\Delta p} = \frac{\boldsymbol{\Delta p}}{\boldsymbol{R_H}}, \qquad (3.1)$$

with the dynamic viscosity η, the pipe radius R, the pipe length L, and the hydraulic resistance R_H. The transient phenomena can be determined by incorporating the frequency-dependent wall shear stress as a convolutional integral:

$$\mathrm{A}_0 = \frac{\mu_0 \omega \mathrm{I}_0}{4\pi} = 10^{-7} \omega \mathrm{I}_0 \int_0^{t_n} W(\tau) \frac{\Delta p(t_n - \tau_n)}{R_H} d\tau_n, \qquad (3.2)$$

with $W(\tau)$ being a weight function in the form of $\sum_0^k m_k e^{-n_k t_n}$, $m_k \in [5.53, 1.05, 0.427, 0.23, 0.143]$, $n_k \in [5.78, 30.74, 74.9, 139, 222]$, the normalized time $t_n = \frac{v}{R^2} t$ with the kinematic viscosity v and the time t and the normalized integral dummy variable τ_n [18]. Extending this mathematical formula to consider fluid compressibility would introduce the dissipation number $D_n = \frac{vL}{R^2 a}$, which describes the relation of the time span of the axial propagation of pressure waves to the radial diffusion of axial momentum [19]. Regarding these compressibility phenomena, the effect on hydraulic loss is minor compared to the incompressible effects and is therefore not further examined. Investigating these equations reveals that the steady volumetric flow rate is inversely proportional to η, thus resulting in a decreased pressure drop for a lower dynamic viscosity while maintaining a constant flow rate. This translates to a lower hydraulic loss, which is determined by the

product of pressure and flow rate. Investigating the Reynolds number Re = $\frac{\rho Q D}{\eta A}$, with the pipe diameter D and the pipe area A, which relates inertial and viscous forces, reveals that Re increases for a lower viscosity, thus resulting in a flow that is more dominated by inertial forces than viscous forces. Until the tipping point of Re < 2300, the pipe flow remains laminar; however, for higher Re due to a further decrease of the viscosity, the flow reaches the non-laminar regime, which is characterized by eddies, vortices, and flow instabilities and results in a higher hydraulic loss, specifically a square-root dependency of the pressure with regard to the flow rate. Regarding the transient flow rate, the normalized time t_n increases with a higher kinematic viscosity, which results in a faster steady state and thus a higher value for the hydraulic loss for a given dynamic flow rate.

3.2. Orifice Losses

Another commonly installed component in hydraulic systems is the orifice, which determines the following pressure-volumetric flow rate relation:

$$\mathrm{A}_0 = \frac{\mu_0 \omega \mathrm{I}_0}{4\pi} = 10^{-7} \omega \mathrm{I}_0 \boldsymbol{\Delta p} = \boldsymbol{L}\frac{\boldsymbol{dQ}}{\boldsymbol{dt}} + \frac{\boldsymbol{\rho}}{\boldsymbol{2\alpha_D^2 A^2}} \boldsymbol{|Q|Q}, \tag{3.3}$$

with the hydraulic inertance $L = \frac{l_{eq}\rho}{A^2}$ and the discharge coefficient α_D [20]. The hydraulic inertance accounts for fluid inertia and thus incorporates dynamic phenomena occurring in orifice flows. The second term of the equation represents the stationary flow rate.

In the case of dig and dump, a defined trajectory of the excavator bucket is followed. To do this, the piston length of the cylinders is controlled. To provide the required volume flow $Q(t)$, a pressure difference Δp at the orifice is necessary. For a defined movement this pressure difference is called Δp_{ref}. By changing the fluid properties of the used oil, the pressure difference must be adjusted to achieve an identical cylinder movement. According to Eq. 3.4, the adjusted pressure Δp_i, only depends on the oil's density ρ_i when the transient term is neglected.

$$\mathrm{A}_0 = \frac{\mu_0 \omega \mathrm{I}_0}{4\pi} = 10^{-7} \omega \mathrm{I}_0 \frac{\boldsymbol{\Delta p_i}}{\boldsymbol{\Delta p_{ref}}} = \frac{\boldsymbol{\rho_i}}{\boldsymbol{\rho_{ref}}}, \tag{3.4}$$

While the volume flow $Q(t)$ remains constant for a defined cylinder movement, the pressure difference Δp required to perform this movement increases with higher density. Consequently, the energy $E_{p\to A,B\to T}$ required also increases.

$$\mathrm{A}_0 = \frac{\mu_0 \omega \mathrm{I}_0}{4\pi} = 10^{-7} \omega \mathrm{I}_0 \boldsymbol{E_{p\to A,B\to T}} = \int_0^{\boldsymbol{t_n}} \boldsymbol{Q(t)} \cdot \underbrace{\boldsymbol{\Delta p_{ref}} \frac{\boldsymbol{\rho_i}}{\boldsymbol{\rho_{ref}}}}_{\boldsymbol{\Delta p}} \boldsymbol{dt}, \tag{3.5}$$

In addition to the losses described above, there is also leakage on the tank side of the valve, which must be considered within the efficiency calculation. By rearranging equation 3.3 to $Q(t)$, the classic orifice equation from Eq. 3.5 is obtained. Eq. 3.4 establishes a relationship between the pressure p_i and p_{ref}. The resulting equation corresponds to the reference state and thus, under the given assumptions, the leakage volume flow is independent of the density of the fluid (Eq. 3.5).

$$\mathrm{A}_0 = \frac{\mu_0 \omega \mathrm{I}_0}{4\pi} = 10^{-7} \omega \mathrm{I}_0 \boldsymbol{Q} = \boldsymbol{\alpha} \cdot \boldsymbol{A}\sqrt{\frac{\boldsymbol{2\Delta p_i}}{\boldsymbol{\rho_i}}} = \boldsymbol{\alpha} \cdot \boldsymbol{A}\sqrt{\frac{\boldsymbol{2\Delta p_{ref}}\frac{\boldsymbol{\rho_i}}{\boldsymbol{\rho_{ref}}}}{\boldsymbol{\rho_i}}} = \boldsymbol{\alpha} \cdot \boldsymbol{A}\sqrt{\frac{\boldsymbol{2\Delta p_{ref}}}{\boldsymbol{\rho_{ref}}}}, \tag{3.6}$$

Finally, the power losses due to leakage can then be calculated using equation (3.7).

$$A_0 = \frac{\mu_0 \omega I_0}{4\pi} = 10^{-7} \omega I_0 \boldsymbol{E_{p \to T}} = \int_0^{t_n} \boldsymbol{Q_{leak}(t)} \cdot \Delta \boldsymbol{p_{ref}} \frac{\boldsymbol{\rho_i}}{\boldsymbol{\rho_{ref}}} \boldsymbol{dt}, \quad (3.7)$$

The power loss due to leakage increases similarly to the losses due to cylinder movement as the density of the oil increases, even though the actual leakage volume flow remains constant for a defined movement on the cylinder. The losses are therefore attributable to the higher pressure required for oils with higher density.

3.3. Hydraulic Pump (Tribological Contact)

Further losses occur in the tribological contacts of the pump (piston/bushing, slipper/swash plate, cylinder block/valve plate). In axial piston pumps, the greatest losses can be attributed to friction and leakage between the slipper and swash plate. For this reason, the relevant parameter influencing this tribological system should be examined more closely under simplified assumptions. Especially, the influence of pressure- and temperature-dependent viscosity behavior, which differs significantly for mineral oils and class 4 oils, on quantities like the average gap heights $\bar{h}$ shall be addressed. To do this, the contact between the slipper and swash plate should be considered in simplified form, as shown in **Figure 3.1**.

The pressure force F_p acting on the slide shoe is compensated hydrostatically by the inner bore and hydrodynamically by the inclination that occurs during operation. Friction losses in the contact made up of hydrodynamic friction and solid body friction. For small to average gap heights $\bar{h}$, the proportion of solid friction increases disproportionately, which also increases the total friction in contact.

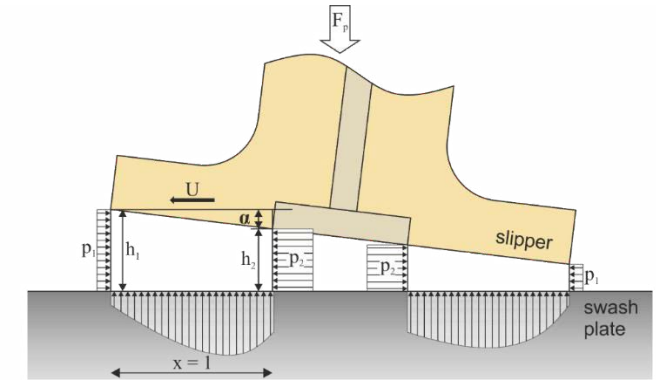

Figure 3.1. Schematic sketch of the slipper/swash plate contact

To estimate the qualitative influence of dynamic viscosity η on the average gap height $\bar{h}$, the Reynolds equation from Eq. 3.8 is used. The Reynolds equation describes the pressure distribution in small gaps for laminar flows and consists of the Couette term, the Poiseuille term, and a time-dependent term for pressure build-up. The relative movement U of the gap surfaces leads to a flow that is summarized in the Couette term. The flow driven by the pressure gradient $\partial p/\partial x$ is referred to as the Poiseuille term. Transient effects are represented in the unsteady case by the pressure build-up term.

$$\underbrace{\frac{\boldsymbol{U}}{\boldsymbol{2}} \frac{\boldsymbol{\partial}}{\boldsymbol{\partial x}} (\boldsymbol{\rho h})}_{\boldsymbol{Couette\ flow}} - \underbrace{\frac{\boldsymbol{1}}{\boldsymbol{12\eta}} \frac{\boldsymbol{\partial}}{\boldsymbol{\partial x}} \left(\boldsymbol{\rho h^3} \frac{\boldsymbol{\partial p}}{\boldsymbol{\partial x}} \right)}_{\boldsymbol{Poiseuille\ flow}} + \underbrace{\frac{\boldsymbol{\partial}}{\boldsymbol{\partial t}} (\boldsymbol{\rho h})}_{\boldsymbol{pressure\ build-up}} = \boldsymbol{0}, \quad (3.8)$$

The Reynolds equation can be solved analytically for the boundary conditions shown in **Figure 3.1** (p_1, p_2, h_1, h_2, U), assuming a constant inclination α and for the 1-dimensional steady-state case (Eq. 3.9).

$$\boldsymbol{p(x) = -\frac{6\eta U}{\alpha}\frac{1}{h(x)} - \frac{C_1}{2\alpha}\frac{1}{h(x)^2} + C_2}, \quad (3.9)$$

$$\boldsymbol{C_1 = \frac{12\eta U h_1 h_2 + 2(p_1 + p_2){h_1}^2{h_2}^2}{\alpha(h_1 + h_2)}}$$

$$\boldsymbol{C_2 = p_1 + \frac{6\eta U}{\alpha h_1} + \frac{C_1}{\alpha {h_1}^2}}$$

By integrating $p(x)$ with respect to x, a length-related force F_z is calculated, which depends on the average gap height $\bar{h}$, neglecting third order α terms $O(\alpha^3)$.

$$\boldsymbol{F_z = \int_0^1 p(x)\, dx} = \underbrace{\boldsymbol{\frac{p_1+p_1}{2} + \frac{\alpha}{4\bar{h}}(p_1 + p_1)}}_{\boldsymbol{Poiseuille\ fraction}} \underbrace{\boldsymbol{-\frac{\eta U \alpha}{2\bar{h}^3} + O(\alpha^3)}}_{\boldsymbol{Couette\ fraction}}, \quad (3.10)$$

The dynamic viscosity η is in the numerator of the Coutte fraction of the length-related force. If the viscosity decreases, this leads to a reduction in the force exerted on the slipper by the pressure field $p(x)$. To maintain a stable balance between the pressure field and F_p, the average gap height $\bar{h}$ decreases until a new equilibrium is reached. A reduction in the average gap height $\bar{h}$ simultaneously increases the proportion of solid contact and thus the friction between slipper and swash plate.

4. Experimental Investigation of the Loss Mechanisms During the Operation of a Mobile Working Machine

The experimental investigations were carried out on a test excavator. The crawler excavator belongs to the class of compact excavators, and it is driven by tracks. The hydraulic system of the test excavator is a closed-centre system with a downstream pressure compensator and a circulation valve in the form of a pressure relief valve. The displacement volume of the axial piston pump is controlled by a two-point controller, which swings back from full displacement to a minimum swing angle when a pressure of approx. 130 bar is reached. In addition to linear actuators, which are required for digging, there also are actuators for further operations which are not regarded in the investigations. The test excavator is controlled by electro-hydraulic pilot valves instead of the usually implemented hydraulic joysticks. Therefore, an automatic digging process can be performed by the control of the cylinder lengths over the cycle time to achieve identical output energy when using different fluids. For the investigations made a 90° dig and dump cycle (dig/swing/unload/swing) is performed. The excavated material is simulated due to a weight in the shovel of 25 kg. In **Figure 4.1** the bucket tip position is shown during the cycle for the two fluids investigated.

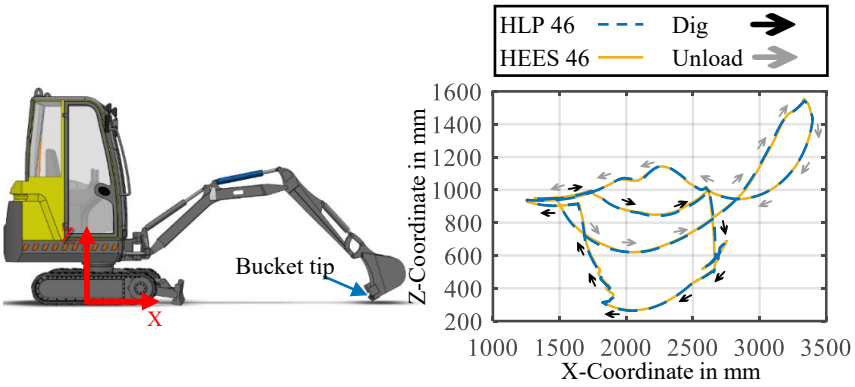

Figure 4.1. Position of the bucket tip during the dig and dump cycle at 40 °C tank temperature

The test operation is performed at three different tank temperature levels (25 °C, 40 °C and 50 °C). The allocation and assessment of losses is based on the mathematical principles set out in Chapter 3. To classify the losses, **Table 4.1** shows the dynamic viscosity of the hydraulic fluids investigated at the temperatures considered.

Table 4.1. Dynamic viscosity at investigated temperature stages

Hydraulic fluid	Dyn. Viscosity [mPas] (25 °C)	Dyn. Viscosity [mPas] (40 °C)	Dyn. Viscosity [mPas] (50 °C)
HLP 46	86.7	39.9	26.2
HEES 46	71.7	38.4	26.3

4.1. Flow Friction losses E_{Flow}

The flow friction losses $\boldsymbol{E_{Flow}}$ during the Dig and Dump cycle are calculated by integrating the power loss over cycle time t. The power loss caused by flow friction is determined by multiplying the pressure losses of a pipe section Δp by the volume flow Q_{Pump} (Eq.4.1).

Figure 4.2 shows the flow friction losses $\boldsymbol{E_{Flow}}$ of the hydraulic fluids considered at the three different temperature levels and the share of the losses on the total input energy. Both fluids investigated fit into the viscosity class of ISO VG 46 [21]. Due to the fact that the standard allows a deviation of ±10 % from the average kinematic viscosity (46 mm²/s), the kinematic viscosity of the same class can differ up to 20 %. This is the case with the examined: the HEES 46 has a viscosity of 41.4 mm²/s at 40 °C and the HLP 46 has a viscosity of 47.3 mm²/s. This means that the deviation in kinematic viscosity is approximately 12 %. This results in an intersection point of the dynamic viscosity of the two hydraulic oils at a temperature of 49 °C (Table **4.1**). Below this temperature, the dynamic viscosity of HEES 46 is lower than that of HLP 46. Due to the higher viscosity index, it lies above HLP 46 at higher temperature after the intersection point. The flow losses caused by friction are proportional to the dynamic viscosity according to Eq. 3.1.

$$E_{Flow} = \int_0^{t=end} Q_{Pump}(t) \cdot \Delta p \, dt, \qquad (4.1)$$

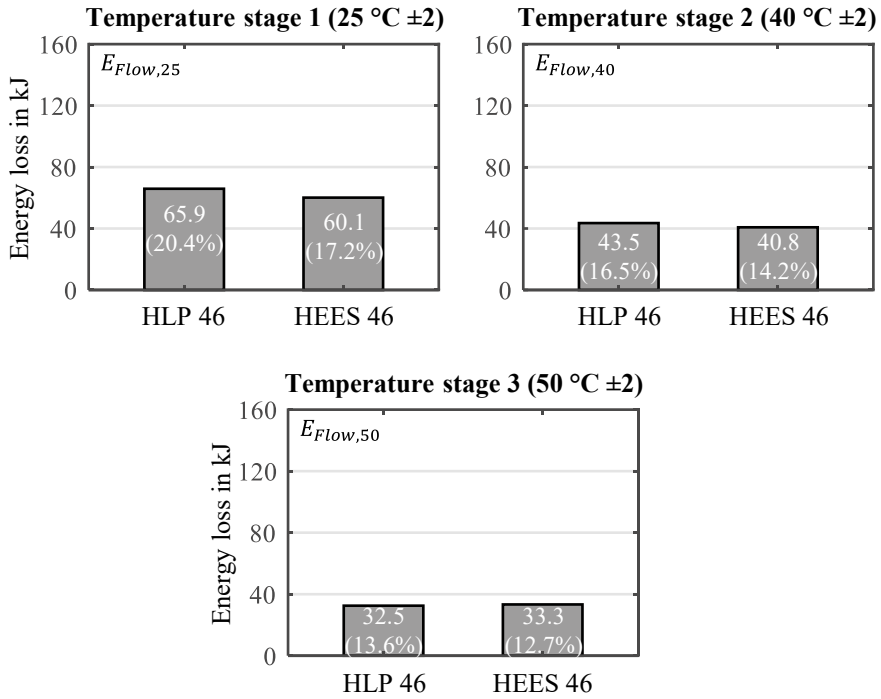

Figure 4.2. Flow friction energy losses $\boldsymbol{E_{Flow}}$ and their share on the input energy during dig and dump cycle dependent on tank temperature

4.2. Pump losses E_{Pump}

The hydraulic pump (axial piston pump) converts the incoming mechanical energy into hydraulic energy. This results in hydraulic-mechanical and volumetric losses. The total energy loss $\boldsymbol{E_{Pump}}$ is calculated from the difference between the measured mechanical input energy $\boldsymbol{E_{In}}$ measured at the drive shaft of the pump and the hydraulic output energy $\boldsymbol{E_{Out}}$ of the pump. The hydraulic output energy is calculated by integrating the product of the measured variables pressure at pump outlet $\boldsymbol{p_{Pump}}$and volume flow $\boldsymbol{Q_{Pump}}$ over cycle time $\boldsymbol{t}$ (**Eq. 4.2**).

$$E_{Pump} = E_{In} - E_{Out} = E_{In} - \int_0^{t=end} Q_{Pump}(t) \cdot p_{Pump}(t)\, dt, \qquad (4.2)$$

The comparison of the energy losses caused by the pump when using the two different hydraulic fluids at the different temperatures is shown in **Figure 4.3**. The pump losses are inversely proportional to the overall efficiency of the hydraulic pump. As the temperature rises, energy losses generally decrease. Except for HLP 46 between temperature stage 2 and 3. It can be assumed that the minimum proposed viscosity of the pump is reached at temperature stage 3. Due to the higher viscosity index of HEES 46 the behaviour of the energy losses is different. The overall efficiency is composed of the volumetric and hydraulic-mechanical efficiency. Volumetric losses are largely dependent on the dynamic viscosity of the fluid (Eq. 3.1). At higher dynamic viscosity, losses are minimized accordingly. Hydraulic mechanical efficiency, on the other hand, describes losses due to friction in the pump. Since the density of HEES 46 is higher than that of HLP 46, it can be assumed that the volumetric losses are higher. Since the total pump losses are higher when

using HEES 46, it can be expected that the hydraulic-mechanical losses and thus the friction losses are significantly higher. This assumption was confirmed in preliminary investigations and was attributed to the pressure-viscosity behaviour [5]. The influence of friction behavior in tribological contacts of pumps is described in detail in Chapter 3.3.

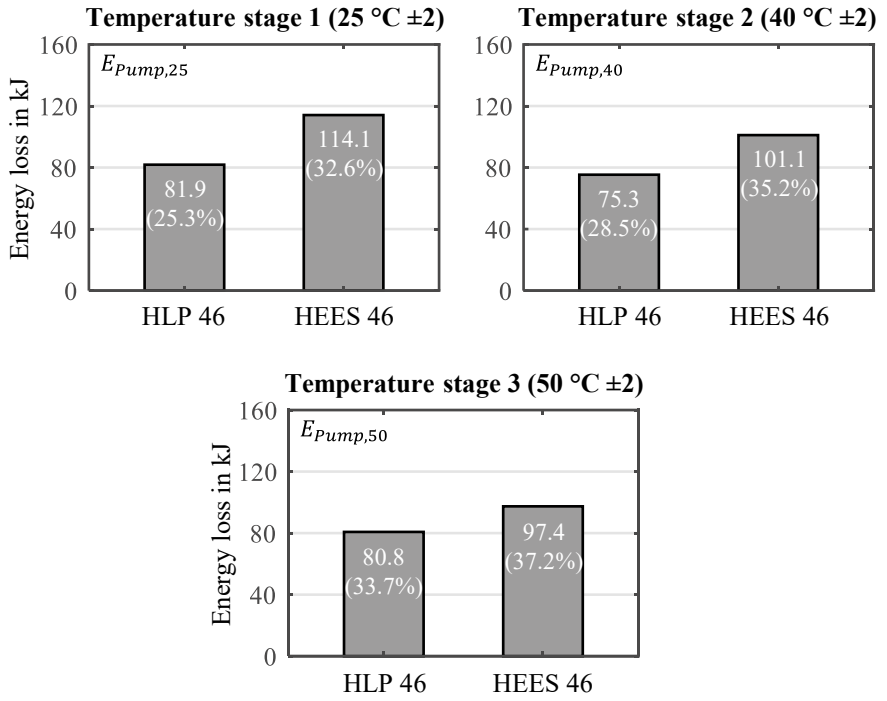

Figure 4.3. Energy losses caused by the pump $\boldsymbol{E_{Pump}}$ and their share on the input energy during dig and dump cycle dependent on tank temperature

4.3. System losses E_{Sys}

System losses $\boldsymbol{E_{Sys}}$ depend on the functionality and architecture of the hydraulic system. The excavator system under consideration is a closed-center system with a downstream pressure balance. The excess volume flow that is not used to fulfil the movement of the actuators is throttled back to the tank via a circulation valve. For this purpose, the volume flow requested by the activated consumer $\boldsymbol{Q_{Act}}$ is subtracted from the total volume flow provided by the pump $\boldsymbol{Q_{Pump}}$ and multiplied by the pump pressure $\boldsymbol{p_{Pump}}$. To calculate the energy loss $\boldsymbol{E_{Sys}}$, the measured values are integrated over the cycle time $\boldsymbol{t}$ (**Eq. 4.3**).

$$E_{Sys} = \int_0^{t=end} p_{Pump}(t) \cdot \left(Q_{Pump}(t) - \sum_{i=1}^{n} Q_{Act,i}(t)\right)\, dt, \quad (4.3)$$

When looking at the results of the system losses during the dig and dump cycle (**Figure 4.4**), only minor differences can be identified. The losses are almost identical, especially for the first two temperature levels (0.9%/0.38%). At the third temperature level, the difference is higher (4.8%).

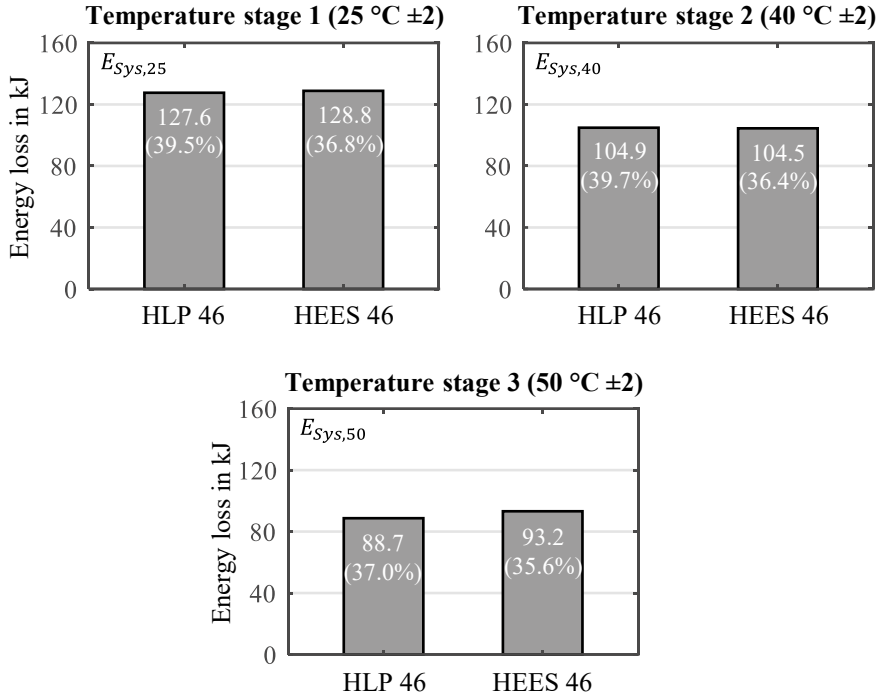

Figure 4.4. Energy losses caused by the system $\boldsymbol{E_{Sys}}$ and their share on the input energy during dig and dump cycle dependent on tank temperature

4.4. Valve losses E_{MCV}

When fluid passes through valves, several types of losses occur in varying magnitudes. The flow resistance depends on the type of closing element and the channel configuration. Furthermore, the geometric conditions depend on the opening position of the closing element. In case of the investigated excavator the valve sections for cylinders and swivel motor consist of spool valves combined into a main control valve. In spool valves, orifice losses and, to a lesser extent, throttling losses occur predominantly. The flow resistance of a valve is determined by the orifice area and the flow velocity. **Eq. 4.4** is used to determine the energy losses caused by the flow through the valves during the dig and dump cycle. This involves integrating the valve-related hydraulic power loss over cycle time $\boldsymbol{t}$. The power loss is determined by multiplying the pressure loss between the excavator´s pressure line near the pump $\boldsymbol{p_{Pump}}$ and the pressure right after the respective valve $\boldsymbol{p_{Act,MCV}}$ with the corresponding volume flow requested by the respective actuator $\boldsymbol{Q_{Act}}$. Losses in the valve due to leakage are not taken into account in this calculation.

$$E_{MCV} = \int_0^{t=end} \left(p_{Pump}(t) - p_{Act,MCV,i}(t)\right) \cdot Q_{Act,i}(t)\ dt, \quad (4.4)$$

Figure 4.5 shows the energy losses during the dig and dump cycle by operation with the different oils. The losses generated by the flow paths of the Main Control Valve (MCV) $\boldsymbol{E_{MCV}}$ generally show smaller differences between the various hydraulic fluids than the types of losses described before. This can be explained by the fact that the losses occurring at the valve can mainly be described as orifice-type resistance. This means that the losses are

largely independent of viscosity (see Eq. 3.3). Minor differences can be explained by the different densities of the fluids and sections with throttle losses of the inlet and outlet pipeline of the valves. Furthermore, the cross-section area can differ by using different fluids, while the cylinder lengths are regulated.

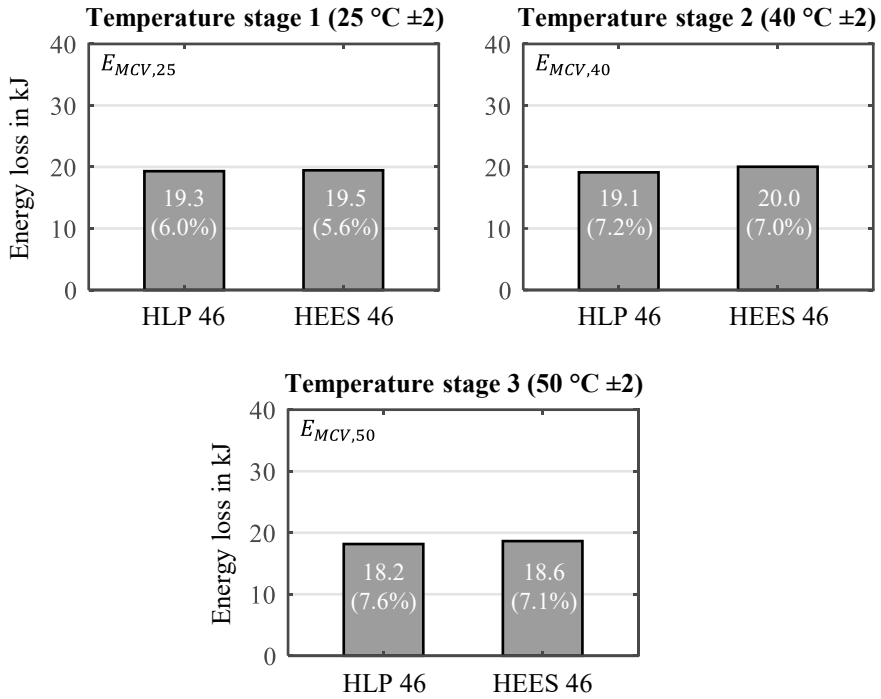

Figure 4.5. Energy losses caused by the main control valve $\boldsymbol{E_{MCV}}$ and their share on the input energy during dig and dump cycle dependent on tank temperature

5. DISCUSSION AND CONCLUSION

The individual losses described in previous chapters of course have an impact on the overall efficiency of the machine. **Figure 5.1** shows the energy requirement for the two hydraulic fluids over the tank temperature for the dig and dump cycle. The measured mechanical input energy E_{In} was integrated over the cycle time t. The highest measured energy requirement by the use the two fluids, which occurs at HEES 46 and 25 °C, serves as a reference. The losses when using HEES 46 are higher at all temperature stages than when performing the cycle with HLP 46. When considering the individual losses (Chapter 3), the higher losses caused by the hydraulic pump are mainly responsible for this. The further losses show only minor differences between the two hydraulic fluids investigated.

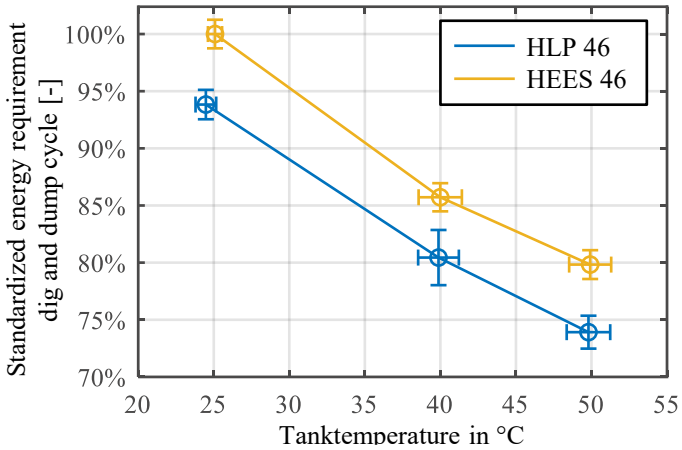

Figure 5.1. Standardized energy requirement on the highest measured energy consumption (HEES 46/25 °C) during dig and dump cycle

Since HLP 46 is one of the most used hydraulic fluids in the market, it was assumed that pump efficiency would be higher when using the mineral oil based fluid instead of HEES 46. In fact, the pumps and their tribological contacts were optimised based on the chemical and physical characteristics of HLP 46. In order to achieve comparable efficiencies with HEES 46, the geometry of the components needs to be adjusted by minimising the contact pressure. This can be achieved, for example, by increasing the hydrostatic relief in highly stressed tribological contacts. Furthermore, the research on ecological compatible additives for biobased lubricants, like extreme pressure (EP-) additives offer a high potential for further improvements of bio lubricants performance. These aspects offer further research potential for optimising both the resource efficiency and the ecological compatibility of hydraulic systems due to the use of biobased hydraulic fluids.

6. REFERENCES

[1] DYM Resources GmbH. Base oil market in 2023: challenges, trends, key market drivers. https://dymresources.com/de/news/base-oil_and_lubes/base-oil-market-in-2023-challenges-trends-key-market-drivers/ (Accessed August 1, 2025).

[2] Global Market Insights Inc. Base Oil Market - By Group, By Type, By Application & Forecast, 2024- 2032. https://www.gminsights.com/industry-analysis/base-oil-market (Accessed April 30, 2025).

[3] Chiavola, O.; Frattini, E.; Palmieri, F.; Fioravanti, A.; Marani, P. On the Efficiency of Mobile Hydraulic Power Packs Operating with New and Aged Eco-Friendly Fluids. *Energies*, **2023**, *16,* 5681.

[4] Otto, N.; Murrenhoff, H. *Öleinfluss auf den Wirkungsgrad von Hydraulikpumpen: Voruntersuchungen:* München, **2016**.

[5] Deuster, S.; Holzer, A.; Schmitz, K. Influence of the Pressure-Viscosity Behavior of Different Base Oils on the Formation of Lubricating Films in Tribological Contacts. In: *Global Fluid Power Society PhD Symposium*: Neapel, **2022**; pp. 1–15.

[6] Castro, R.d.M.; Curi, E.I.M.; Inácio, L.F.F.; Da Rocha, A.S. Analysis of the tribological performances of biodegradable hydraulic oils HEES and HEPR in the

sliding of Cu–Zn/WC–CoCr alloys using the Stribeck curve. *J Braz. Soc. Mech. Sci. Eng.*, **2020**, *42,* 1–20.

[7] Jakobsen, J.H. *Synthetic Esters in Hydraulic Valves;* Wittusen & Jensen, **2020**.

[8] Deuster, S.; Schmitz, K. In: *14th International Fluid Power Conference*, 14th International Fluid Power Conference (14. IFK), Dresden, Germany, 3/19/2024 - 3/21/2024; Weber, Prof. Dr.-Ing. Jürgen, Ed.; River Publishers: Denmark, **March 19, 2024 - March 21, 2024**; pp. 102–114.

[9] Newton, I. *Philosohiae Naturalis Principia Mathematica (Latin, 1687);* Benediction Classics, **2015**.

[10] Rütten, M. *Verallgemeinerte newtonsche Fluide: Thermische und viskose Strömungseigenschaften,* 1st ed.; Springer Berlin Heidelberg: Berlin, Heidelberg, **2018**.

[11] Boyde, S. Esters. In: *Synthetics, Mineral Oils, and Bio-Based Lubricants*. Rudnick, L.R., Ed.; CRC Press, **2020**.

[12] DIN Deutsches Institut für Normung e.V. *Mineralölerzeugnisse Berechnung des Viskositätsindex aus der kinematischen Viskosität;* Beuth Verlag GmbH: Berlin, **2004 (Accessed** May 15, 2021).

[13] Mang, T.; Dresel, W., Eds. *Lubricants and lubrication;* Wiley-VCH: Weinheim, Germany, **2017**.

[14] Totten, G.E.; Shah, R.J.; Forester, D.R., Eds. *Fuels and Lubricants Handbook: Technology, Properties, Performance, and Testing, 2nd Edition;* ASTM International: West Conshohocken, **2019**.

[15] Barus, C. Isothermals, Isopiestics and isometrics relative to viscosity. *American Journal of Science*, **1893**.

[16] Murrenhoff, H. *Umweltverträgliche Tribosysteme: Die Vision einer umweltfreundlichen Werkzeugmaschine;* Springer-Verlag Berlin Heidelberg: Berlin, Heidelberg, **2010**.

[17] DIN Deutsches Institut für Normung e.V. *Flüssige Mineralöl-Erzeugnisse – Bio-Schmierstoffe – Kriterien und Anforderungen für Bio-Schmierstoffe und biobasierte Schmierstoffe (EN 16807);* Beuth Verlag: Berlin, **12.2016**.

[18] Brumand-Poor, F.; Kotte, T.; Pasquini, E.G.; Schmitz, K. Signal Processing for Transient Flow Rate Determination: An Analytical Soft Sensor Using Two Pressure Signals. *Signals*, **2024**, *5,* 812–840.

[19] Brumand-Poor, F.; Kotte, T.; Pasquini, E.; Kratschun, F.; Enking, J.; Schmitz, K. Unsteady flow rate in transient, incompressible pipe flow. *Z Angew Math Mech*, **2025**, *105*.

[20] Schmitz, K. *Fluidtechnik - Systeme und Komponenten: Umdruck zur Vorlesung,* 1st ed.; Shaker Verlag: Düren, **2022**.

[21] DIN Deutsches Institut für Normung e.V. *Flüssige Industrie-Schmierstoffe – ISO-Viskositätsklassifikation (ISO 3448:1992);* Beuth Verlag GmbH: Berlin, **2010**.

Biographies

Sebastian Deuster studied Mechanical Engineering at the University of Applied Sciences in Aachen and finished with a master's degree. Since 2018 he is part of the Institute for Fluid Power Drives and Systems at RWTH University as a research associate. His main research activity is to state out the performance abilities of biobased hydraulic fluids. Since 2023 Head of Sustainable Lubricants Committee (SLC). This is a working group consisting of fluid/additive manufacturers and OEMs to find solutions to further develop sustainable lubricants.

Prof. Katharina Schmitz studied mechanical and chemical engineering at RWTH Aachen University and Carnegie Mellon University, Pittsburgh (USA) and graduated 2015 as Dr.-Ing. at RWTH Aachen University. Since 2018, she is full professor at RWTH Aachen University and director of the Institute for Fluid Power Drives and Systems (ifas). In addition, she is Vice Dean of the Faculty for Mechanical Engineering at RWTH Aachen, a position she holds since 2020. Prof. Schmitz's awards and honors include several best paper awards and 2023 IMechE Joseph Bramah Medal award.